RSC Advances

PAPER

View Article Online
View Journal | View Issue

Cite this: *RSC Adv.*, 2016, **6**, 68292

Surface and interface reaction analysis of Zr films deposited on 6H-SiC after thermal annealing

E. G. Njoroge,* C. C. Theron, T. T. Hlatshwayo and J. B. Malherbe

Received 20th May 2016
Accepted 11th July 2016

DOI: 10.1039/c6ra13119k

www.rsc.org/advances

Zr films (130 nm) were deposited on a 6H-SiC substrate at room temperature by sputter deposition. The interface solid-state reactions due to high vacuum thermal annealing between 600 °C and 850 °C for 30 min were investigated by Rutherford backscattering spectrometry (RBS) and X-ray diffraction (XRD). The surface morphology evolution due to thermal annealing was investigated and quantified using atomic force microscopy (AFM) and secondary electron microscopy (SEM). RBS analysis indicated that the as-deposited sample had a thin intermixed region consisting of ZrC and Zr_2Si. The phases formed at each temperature were identified by XRD analysis. At temperatures of 700 °C and above, Zr reacted with the SiC substrate and formed a mixed layer of Zr carbide (ZrC) and Zr silicides (Zr_2Si, $ZrSi_2$ and Zr_5Si_3). The surface morphology from SEM analysis revealed a homogeneous Zr surface which varied with annealing temperature with the appearance of clusters on the Zr surface. AFM analysis revealed that the R_{RMS} surface roughness decreased from the as-deposited value of 1.65 nm after annealing at 700 °C and then increased at higher temperatures due to coalescing of the surface granules in the Zr layer. It has also been demonstrated that the obtained experimental results between Zr and SiC have a good correlation with the ternary EHF model with regards to initial phases formed in the interface.

1. Introduction

Silicon carbide is a ceramic and a semiconductor material that has a wide range of applications due to its excellent properties. These include good mechanical wear resistance, high thermal conductivity, chemical attack resistance, high melting point, high thermal stability, a high hardness value, and high radiation damage resistance (also with a low neutron absorption cross-section).[1–5] Due to these attractive properties, SiC has been applied as a structural material, also in modern nuclear fuel, and in electronic devices.[6–8]

SiC is used as the main barrier which acts to retain fission products (FP) in tri-structural-isotropic (TRISO) particles used in high temperature gas cooled reactors (HTGRs) such as the pebble bed modular reactor (PBMR).[9–12] The SiC layer also provides structural integrity to the fuel pellet and act as a barrier against cooling gas contamination under reactor operation and fuel storage conditions.[12] The Zr yield in most nuclear fuels has been found to be high compared to other fission products.[10] Zirconium is a transition metal with a high melting point (1850 °C) and is also ductile. This metal has been proposed for use in metal matrix microencapsulated (M3) fuels being developed for use in light water reactors (LWRs).[13,14] M3 fuel consists of TRISO or bi-structural isotropic (BISO) fuel particles embedded in a Zr metal matrix to form an integral fuel rod. The fabrication processes of M3 rods involve hot pressing, hot isostatic pressing (HIP) and extrusion techniques using coarse Zr power with TRISO and BISO particles dispersed in the matrix. These fabrication processes could lead to solid-state interactions from material interdiffusion across the fuel–metal interface. These interactions could lead to failure of the M3 fuel rod.

SiC has been considered for use as a reinforcement material in metal matrix composite materials.[13] These composite materials such as Zr/SiC, have been proposed as a possible fuel structure for high temperature reactors (HTR) with the aim of reducing the Zr metal fraction in the composite, while maintaining a neutronic behaviour very close to the Zr one.[15,16] These metal matrix composites have a high SiC content, therefore increasing the surface area available for Zr/SiC interactions. Zr has also been proposed as a stable metal contact to SiC for high temperature electronic operations.[17]

In the above mentioned applications, SiC is in contact with Zr at high temperatures and the performance of these structures depends greatly on the stability of the Zr/SiC interface. In TRISO fuel particles, these interactions can lead to the reduction in thickness of the SiC layer with the formation of undesired reaction products or provide localized fast diffusion paths for other FPs. This can degrade the capability of retaining FPs within the particle and limit the fuel lifetime at higher temperatures therefore leading to safety and performance limitations of TRISO fuel particles. In metal matrix composites, interface reactions are bound to occur at elevated temperatures and may lead to adhesion–cohesion failure at the Zr/SiC

Department of Physics, University of Pretoria, Pretoria 0002, South Africa. E-mail: eric.njoroge@up.ac.za; Tel: +27-12-4204777

This journal is © The Royal Society of Chemistry 2016

interface during processing and application stages. This ultimately leads to microstructural changes which may result in changes in material properties and reduction in strength of the composites.

The solid-state reactions between a metal and SiC are usually governed by thermodynamics and the reaction kinetics of the metal/SiC system. The thermodynamic factors determine which phases can appear at the interface during the processing and service conditions while the kinetics determine how much of a phase can be formed.[18] The main driving force in thermodynamics case is usually the reduction of the Gibbs free energy of the system due to chemical reactions.[19] This usually determines if a reaction between a metal and SiC can occur at elevated temperatures.

The binary effective heat of formation (EHF) model developed by Pretorius *et al.*[20] was extended to ternary systems by Mogilevsky and Gutmanas.[21] In the case of ternary systems, the two dimensional EHF diagrams are replaced by corresponding three dimensional constructions where the tetrahedral replace the binary EHF triangles. From these three dimensional representations, maps of favourable reaction products can be drawn. The EHF model has been applied to metal/SiC systems including Ta/SiC, Ti/SiC and Nb/SiC by Mogilevsky and Gutmanas[21] but it has not been previously assessed if it can be applied to the Zr/SiC system. These metals form both silicides and carbides with SiC and the initial phases to form in these ternary systems were predicted to good accuracy.

Previous studies on the Zr/SiC involved the use of bulk Zr metal in contact with SiC and investigated the kinetics, microstructure and thermodynamics.[22–26] In this paper, the stability between Zr layer and SiC substrate, initial temperature of reaction, interface reactions, surface topography, initial phases formation and phase evolution under vacuum annealing between 600 and 850 °C were investigated by Rutherford backscattering spectrometry (RBS), X-ray diffraction (XRD), secondary electron microscopy (SEM) and atomic force microscopy (AFM). The ternary EHF model was applied and the initial phases to form in the Zr/SiC interface predicted and compared with the experimental results.

2. Experimental method

Zr films were sputter deposited on 6H-SiC substrates using an AJA International Inc. Orion 5 sputtering system. The Zr sputtering target (AJA International Inc.) was 50.8 mm in diameter and 6.35 mm thick with 99.5% purity. The semi-insulating SiC wafers (Pam-Xiamen) were single-face polished with Si face epiready, 50.8 mm diameter, 330 μm thick, micro pipe density of <30 cm^{-2} and with root mean square (RMS) surface roughness of less than 0.5 nm. The wafers were cleaned by a chemical treatment to remove any contamination and the native oxide layer. This involved degreasing the SiC substrates in an ultrasonic bath for 5 minutes for each step, in trichloroethylene, acetone and methanol, followed by rinsing in deionised water after each stage of chemical cleaning. The samples were then dipped in 10% HF to remove the oxide layer on SiC then rinsed in deionised water and blow dry using nitrogen gas. The Zr target (DC sputtering) and the SiC (RF sputtering) substrate were sputter-cleaned for 10 minutes using Ar plasma before the room temperature sputtering was done. This ensured the removal of the native oxide layer from the SiC wafer and a clean Zr target surface for sputtering, since Zr readily oxidizes in air. These samples were annealed between temperatures of 600 and 850 °C for durations of 30 minutes under high vacuum conditions (<$\times 10^{-6}$ mbar). All the samples were analysed by Rutherford backscattering spectrometry (RBS) before and after annealing. The energy of the He^+ ions was 1.6 MeV with a scattering angle of 165° with the sample tilted 10° off the normal. RBS analysis was performed to obtain the elemental composition of the as-deposited and annealed samples, the thickness of deposited Zr film and the thickness of the reaction zone.

The X-ray diffraction (XRD) analysis was performed using a Bruker D8 Advanced XRD system with a Cu (K_α) radiation source ($\lambda = 0.1540598$ nm) at two-theta step size of 0.04°. This was done to identify the phase formation and orientation before and after annealing of the samples using the International Centre for Diffraction Data files (ICDD-PDF-2) database. Surface morphologies were examined by SEM using a Zeiss Ultra 55 field emission scanning electron microscope. This was done at low beam energy of 2 kV to reveal surface features before and after annealing. The AFM images were obtained using the Dimension Icon AFM system, working in contact mode in an air ambient. The AFM images were obtained and analysed using NanoScope Analysis offline software. In this study, the AFM images analysed were of 2 × 2 μm scan sizes for the as-deposited and annealed samples.

3. Results and discussion

The RBS spectrum of the as-deposited Zr/SiC sample is displayed in Fig. 1 along with the simulated spectrum obtained

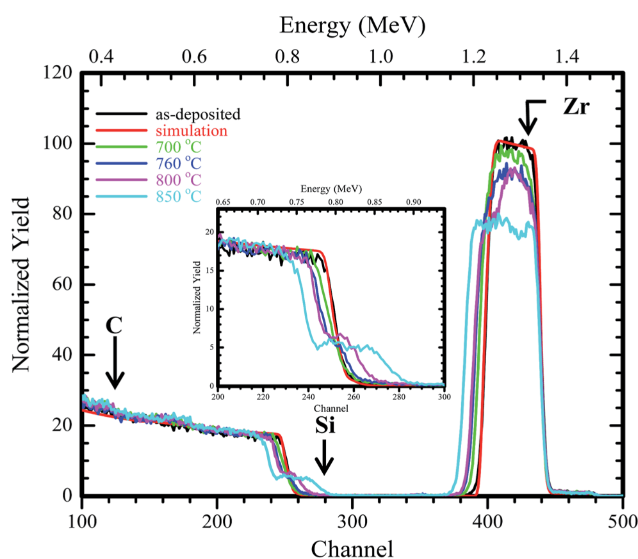

Fig. 1 Raw RBS spectra of as-deposited Zr/SiC and samples annealed at 700, 760, 800 and 850 °C. The RUMP simulation spectrum of as-deposited has been included.

using the RUMP computer code.[27] The arrows in the graph shown in Fig. 1 indicate the surface positions of Zr, Si and C at channel numbers 440, 289 and 117 respectively. The as-deposited Zr film exhibits a step starting at channel number 479; this is attributed to hafnium which inherently occurs in Zr metal in trace amounts. From the RUMP simulations, the HF concentration in the deposited layer was found to be about 0.2%, which is close to the manufacturer's stated level of 0.3%. The thickness of the as-deposited Zr film was calculated from RBS spectra from RUMP simulations and was found to be 130 nm. Although the Zr low energy edge and Si high energy edge was observed to be flat indicating that the deposited Zr had a sharp interface with the SiC substrate, a thin intermixed layer of about 40×10^{15} at. per cm^2 wide had to be included in the as-deposited sample in order to fit the back edge of the Zr peak and Si front edge.

RBS analysis was done on annealed samples to investigate the interactions between Zr and SiC. The RBS spectra of the as-deposited and sample annealed at 600 °C differ insignificantly and hence are not reported here. The simulation of this sample reveals that the Zr layer does not react with SiC after annealing at this temperature.

The overlay of RBS spectra from the as-deposited and annealed samples at 700, 760, 800 and 850 °C for 30 minutes are given in Fig. 1. A reduction in the Zr peak height can observed with increasing annealing temperature compared to as-deposited spectrum. After annealing, the back edge of the Zr signal has a progressive shift towards lower energy channels which increases with temperature. A step was observed to form at the high energy Si edge which grew wider with annealing temperature indicating a growing reaction zone. This implies that interdiffusion is taking place at the Zr/SiC interface. The relative amount of Zr in the interdiffusion zone is higher than the amount of Si and C from RUMP simulation, although the amount of Si and C is the same. These results indicate that the Zr/SiC interface begins to react at temperature of 700 °C with the formation of zirconium carbide and silicides. For reactions to occur at the interface, SiC has to dissociate to its elemental constituents, that is, carbon and silicon.[28] This dissociation of SiC can be catalytically enhanced by the reaction with a metal, because the accepted dissociation temperature of SiC is 2700 °C.[9] After dissociation, C and Si then diffuse from the interface into the Zr metal and Zr diffuses from the interface into SiC to form reaction products.

Annealing at 760 °C for 30 minutes, it is observed from Fig. 1 that the step on the Si edge continues to grow towards the Si surface channel position and deeper into the substrate, indicating lateral growth of the reaction zone. The simulation of the RBS spectrum of the sample annealed at 760 °C was done in terms of a two-layer reaction zone. The thickness of the layer next to Zr was 60×10^{15} at. per cm^2 wide comprising of 67.4% Zr, 12.7% silicon and 19.6% carbon. The layer next to SiC was 285×10^{15} at. per cm^2 wide comprising of 58% Zr, 21% silicon and 21% carbon. These compositions indicate the formation of Zr_2Si and ZrC phases in the reaction zone. Zr surface oxidation can be observed after annealing at 760 °C on high energy edge of Zr peak accompanied with the appearance of the oxygen peak superimposed on the Si signal. The annealing was done in vacuum, with base pressure before annealing in the order of 1×10^{-8} mbar, and during annealing increased to 1×10^{-6} mbar. The strong chemical affinity of Zr for oxygen resulted in gettering the small amount of oxygen present in the vacuum system during annealing.

The step on the low energy side of Zr peak is more pronounced after annealing at 800 °C as seen in Fig. 1. The low energy edge of the Zr peak was observed to shift to lower energy channels indicating interdiffusion at the Zr/SiC interface. The Si step is also observed to grow wider and shifted further into the Zr film after annealing at this temperature. The simulation for the sample annealed at 800 °C was performed with a three layer reaction zone. The thickness of the layer next to unreacted Zr was 100×10^{15} at. per cm^2 wide comprising of 71.3% Zr, 28.5% Si. The next layer was found to be 140×10^{15} at. per cm^2 wide comprising of 60% Zr and 39.5% Si. The third reaction zone layer was 200×10^{15} at. per cm^2 wide comprising of 49.5% Zr, 29.8% Si and 20.7% C. The compositions obtained from RUMP simulations, suggest the formation of Zr_2Si, ZrC and $ZrSi_2$ phases in the reaction zone. The ZrC_x phase formed next to the SiC substrate after annealing at this temperature.

The Si step gets wider with increase in annealing temperature up to 850 °C as seen in Fig. 1. At this temperature, a plateau appears at the top of the Zr signal. The simulation of samples annealed at 850 °C is more complicated and has to be fit with multiple reaction zone layers of different thickness and compositions in order to obtain a good fit. Such fitting with multiple reaction zone layers is fraught with uncertainties depending on the assumptions made. Therefore, the individual layer compositions as obtained from such a fitting are not given. The comparison of the Zr peak total areal counts of the as-deposited with the annealed samples was found to remain relatively constant. This indicates that there was no loss of deposited Zr atoms due to delamination during the annealing process.

The reaction zone growth was characterized with slow reaction rates between 700 and 800 °C as seen in Fig. 2. At higher annealing temperature of 850 °C very fast interdiffusion is

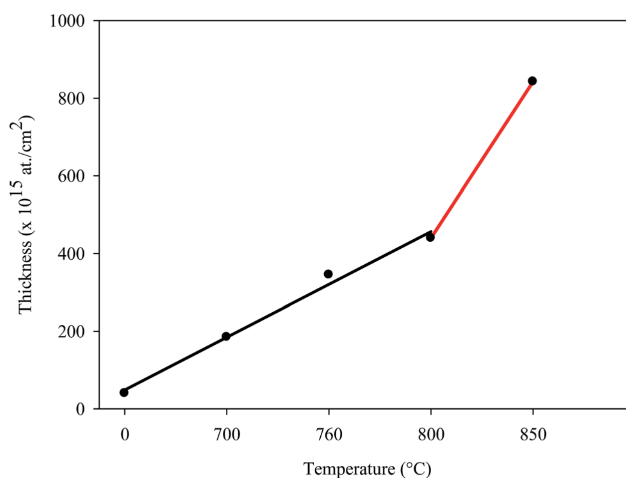

Fig. 2 Isochronal annealing graph. The straight line represents a least square fitting to the data between 0 and 800 °C. The reason for the deviation at 850 °C is discussed in the text.

This journal is © The Royal Society of Chemistry 2016

observed and the reactions occur very rapidly leading to high reaction rates. This can be attributed to the α to β-Zr transformation[29] which occurs at about 860 °C (within margin of experimental errors). At this temperature the self-diffusion coefficients of Zr can change by two orders of magnitude leading to very fast reaction rates.

Fig. 3 shows XRD diffraction patterns of the as-deposited Zr films on 6H-SiC substrate and of samples annealed from 700 to 850 °C for 30 minutes. The diffraction pattern of the as-deposited sample (Fig. 3(a)) revealed peaks of Zr, ZrC, Zr_2Si and SiC substrate. A low intensity α-Zr (hexagonal) peak was observed at $2\theta = 31.9°$ position with (100) orientation plane. The strongest reflections are due to the predominant peaks of the SiC substrate at two-theta 35.78° and 75.47° positions. This also confirmed that the SiC wafer from Pam Xiamen was hexagonal 6H-SiC polytype with lattice constants $a = 3.073$ and $c = 15.08$ Å. Additional peaks were also observed and these were indexed to the (111) and (222) planes of cubic ZrC. Another peak at 34.26° was indexed to hexagonal ZrO_2 which was present due to surface oxidation of the Zr film. It was suspected that the Zr films were oxidizing from RBS analysis and this was confirmed later by XRD analysis with the presence of ZrO_2 from surface oxidation of the Zr layer.

After thermal annealing, some crystalline phases were observed to be forming at the Zr/SiC interface as seen in Fig. 3. The sample annealed at 700 °C (Fig. 3(b)), a Zr peak with higher intensity can be observed revealing the formation of a larger crystallite Zr layer after annealing. In the 35.78° and 75.47° two theta regions, the XRD scan of the 700 °C annealed sample contains peaks corresponding to diffraction from the hexagonal SiC phase. These peaks are also observed at the same two-theta positions in the subsequent annealed samples. Peaks indexed to Zr, ZrC, Zr_2Si and ZrO_2 phases were also observed in the sample annealed at 700 °C for 30 minutes. The diffraction pattern of the 760 °C annealed sample (Fig. 3(c)) contains Zr carbide and silicides peaks corresponding to diffraction from planes of the ZrC (111), ZrSi (020), $ZrSi_2$ (241), Zr_2Si (211) and (332) phases. Other peaks are indexed to Zr from planes (100) and ZrO_2 (004) are also observed in Fig. 3(c). The formation of Zr_2Si, ZrC and $ZrSi_2$ at the interface of this sample correlates with the results obtained from RBS. The formation of ZrC was accompanied by the formation of Zr silicide phases in order to satisfy mass balance after annealing at this and higher temperatures. The only difference (700 and 760 °C) is the ZrC peak appearing at 68.18° two theta position indexed to (222) plane.

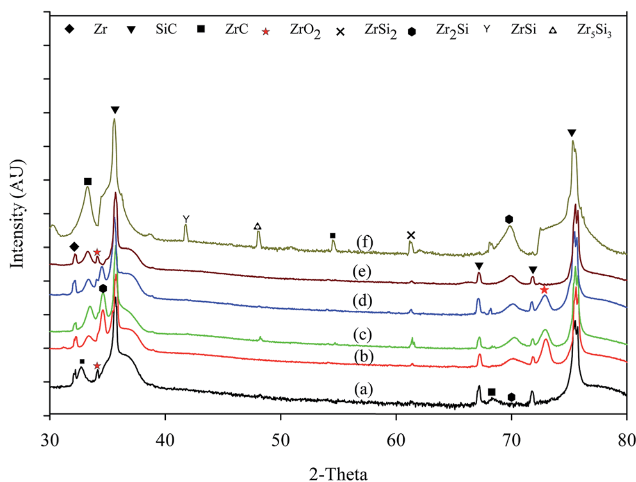

Fig. 3 Overlay of XRD diffraction patterns of (a) as-deposited, samples annealed for 30 minutes at (b) 700, (c) 760, (d) 800, (e) 850 °C and (f) 850 °C for 240 minutes.

The XRD diffraction pattern of the sample annealed at 800 °C for 30 minutes (Fig. 3(d)) contains similar phases to the sample annealed at 760 °C for 30 minutes. From the XRD scan of Zr layer on SiC annealed at 850 °C for 30 minutes (Fig. 3(e)), unreacted Zr can still be observed to be present. The reaction phases observed to have formed include ZrC, $ZrSi_2$ and Zr_2Si.

For the sample annealed at 850 °C for 4 hours (Fig. 3(f)), no unreacted Zr was visible. The various Zr silicide and carbide phases, namely; Zr_2Si, ZrSi, Zr_5Si_3 and ZrC were observed to be present as seen in Fig. 3 showing a dramatic change in the interface structure. The ZrO_2 phase observed to form was due to surface oxidation of Zr. As the reaction zone thickness increased, the evolution of compound formation became more complex as a function of annealing temperature at 850 °C as seen in Fig. 3. No peak-shift neither peak-widening was observed to occur to any of the peaks with increase in annealing temperature. Due to the randomly oriented polycrystalline nature of the deposited Zr layer the phases formed in the reaction zone were in small quantities. These have low peak intensity and poor peak-to-background ratios. Other peaks due to the Zr layer, Zr silicides and carbide were overshadowed or superimposed by the 35.78° peak due to the SiC substrate.

The micro and nano-structure surface morphology analysis of the Zr/SiC as-deposited and annealed sample's surface was analysed by SEM and AFM techniques. The SEM micrographs of representative surface morphologies are shown in Fig. 4 and 5. The uniform deposition can be observed from the low magnification image in Fig. 4(a) which shows a uniform and smooth surface which is almost featureless. At higher magnification, the granular Zr surface is clearly visible as seen in the high magnification image in Fig. 4(b). The sputter deposition of a Zr layer onto the 6H-SiC surface at room temperature resulted in a granular surface which is due to columnar type of growth of the film. It can be observed from these SEM images that the granules on the as-deposited film are uniformly distributed and have nearly the same size. The granules are closely packed and the SiC substrate is fully covered by the Zr layer. There is clear absence of pores and other surface defects in the film.

Although the XRD results indicated slightly larger Zr crystallites after annealing at 700 °C for 30 minutes, this was not evident in the SEM images of the surface with the surface grains becoming smaller in size as seen in Fig. 5(a). Annealing at 760 °C resulted in some of the Zr granules to agglomerate into island clusters and with the remaining grains to be larger in size. The surface of the films annealed at 760 °C and higher temperatures became rougher. A comparison between the SEM micrographs of the as-deposited with the 800 and 850 °C annealed samples indicates the agglomeration of surface

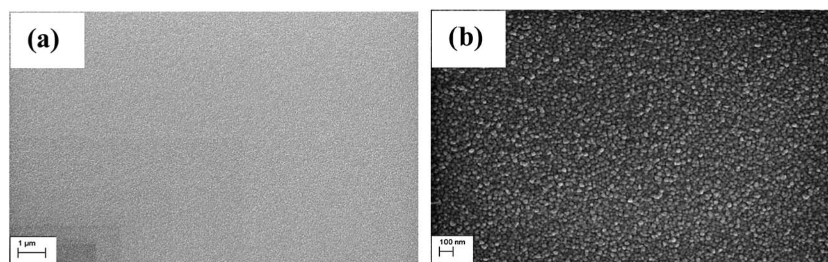

Fig. 4 In-lens SEM images of the surface of as-deposited 130 nm Zr film (a) wide area and (b) high magnification images.

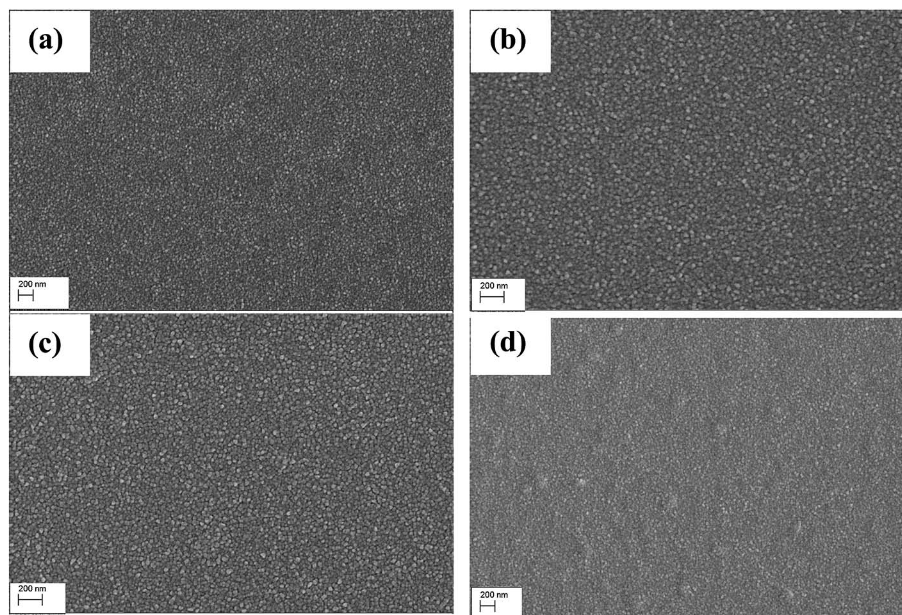

Fig. 5 SEM images of the Zr surfaces annealed at (a) 700 °C (b) 760 °C (c) 800 °C and (d) 850 °C for 30 minutes.

granules into clusters which cause the appearance of hillocks. The rough topography of the surface indicates that substantial reaction and migration at the surface and interface has occurred. The lateral granule diameter on this film is almost uniform over the surface.

AFM characterization and analysis allows for the quantitative analysis of the surface morphology of the Zr films. AFM measurements were performed on the Zr/SiC diffusion couples in order to investigate the influence of the annealing temperature on the surface morphology evolution and roughness characteristics of the deposited Zr layer. The roughness data was obtained from the 2D AFM images using the NanoScope offline analysis software. The as-received 6H-SiC wafer (Fig. 6(a)) is characterized by periodic and parallel terraces with an average height of 1.54 nm which corresponds to six SiC bilayers in a direction perpendicular to the surface (*c* axis). This substrate has an R_{RMS} roughness value of 0.35 nm, therefore minimal SiC substrate roughness was expected to be propagated through the deposited layer up to the surface.

The as-deposited films revealed an evenly distributed granular layer similar to the SEM images. As shown in Fig. 6(b), we can observe from 3D AFM images that the film had Zr granules which indicate that the film was deposited in a column growth process by sputter deposition. The images show a surface that is homogenous and made up relatively small granules with a diameter of 26.61 nm and R_{RMS} roughness of 1.65 nm indicating a smooth surface.

The 2D AFM images (Fig. 6(c)) of samples annealed at 700 °C for 30 minutes display granules of different sizes which are evenly distributed on the sample surface. The average size of the granules can be observed to have reduced to 19.8 nm. The R_{RMS} roughness value of 1.48 nm is lower than the as-deposited one in line with the SEM images. This decrease is due to rearrangement of granules on the Zr/SiC sample surface. After annealing at the temperature of 760 °C, there is a distinct change of the surface structure as observed in Fig. 6(d). The mean granule diameter and R_{RMS} values increased to 20.2 nm and 2.22 nm respectively. A few clusters can be observed on the annealed films; these have considerably larger height compared to the other surface features, the granules. The increase in the R_{RMS} is due to the interfacial reaction, with zirconium silicides and carbide forming at the interface, thereby, restructuring the

 This journal is © The Royal Society of Chemistry 2016

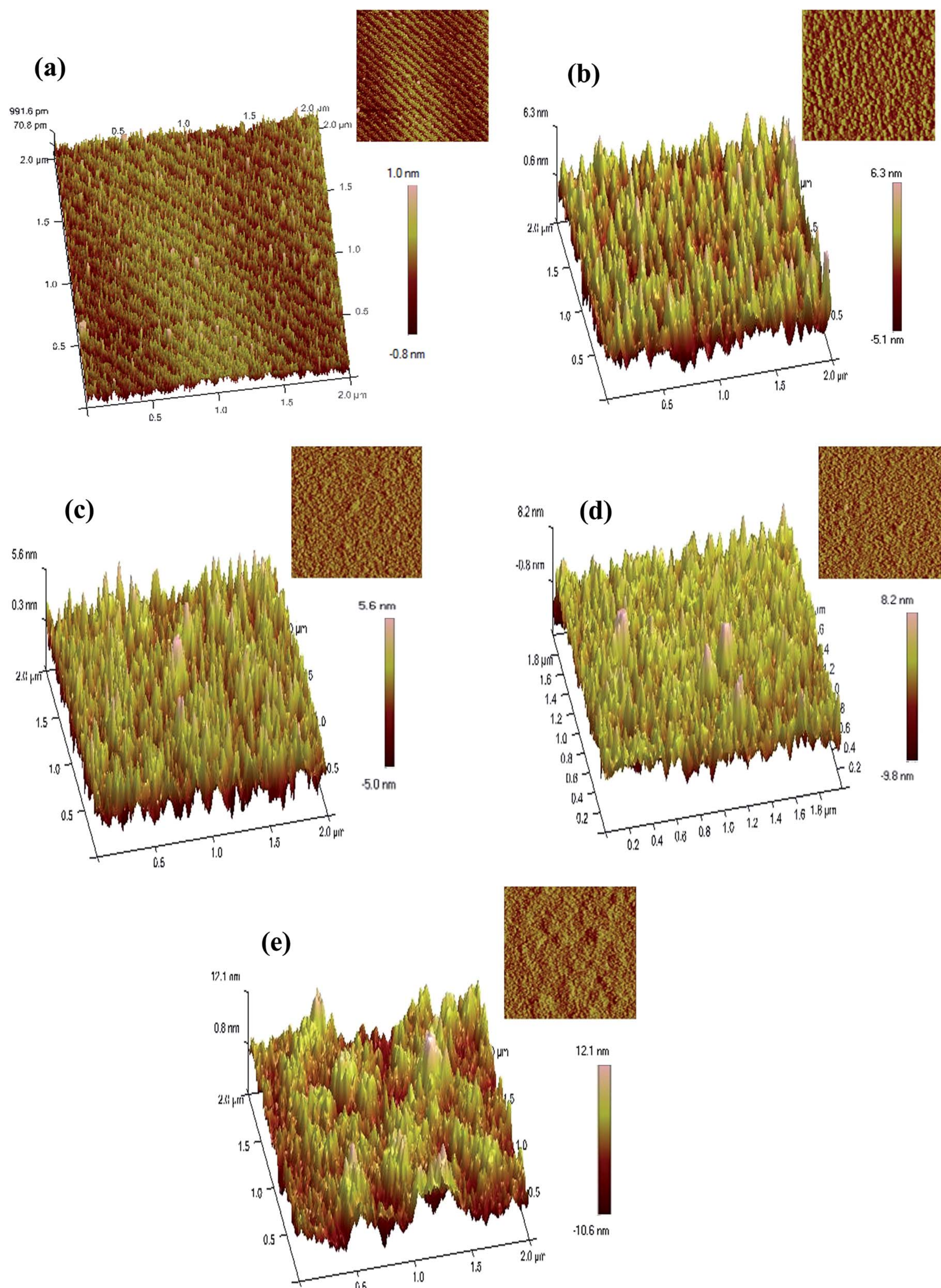

Fig. 6 AFM surface topography images of (a) as-received 6H-SiC substrate with periodic arrangement of terraces which have a height of 1.5 nm, (b) as-deposited Zr films on 6H-SiC and samples annealed at (c) 700 °C (d) 760 °C and (e) 850 °C.

interface. The R_{RMS} values of samples annealed at 850 °C (Fig. 6(e)) show a further increase 3.13 nm (the highest value for all our samples) with a mean granule diameter of 22.0 nm. It can be deduced from the 3D images that the roughness parameter R_{RMS} values increased with the increasing height of the hillocks.

As can be seen in Fig. 7, at annealing temperatures above 700 °C, the R_{RMS} values increased with increase in temperature. Furthermore, from the SEM and AFM images it can also be seen that the density of the clusters also increased. This can be attributed to the coalescing or aggregation of the surface granules into large clusters with increasing annealing temperature as well as the phase formation on the surface at the higher annealing temperatures. The increasing cluster size was seen to influence the surface morphology evolution of the film surfaces, that is, with increasing size and number of clusters, the rougher the surface appears to become. The increase of roughness at annealing temperatures higher than 700 °C corroborates the results obtained with the SEM micrographs. It can be deduced that the surface topography strongly depends on the temperature of anneal.

At higher temperatures, the atoms have enough activation energy to occupy the correct sites in the crystal lattice and granules with lower surface energy become larger. The granules grow in lateral and vertical dimensions is due to the coalescing of the surrounding granules of smaller size.[30] The agglomeration of material on the surface is a material transport process, that is mainly caused by grain boundary diffusion, interface diffusion, surface diffusion or phase transformations.[31] The driving force for the agglomeration is the tendency of thin films trying to reduce the surface-to-volume ratio while the film is approaching its lowest energy state at equilibrium.[32]

The SEM and AFM results indicate that further agglomeration of the surface granular features occurs after annealing at 800 and 850 °C resulting in hillocks and valleys. The surface roughening was observed to originate from agglomeration of granules which are more visible after annealing at 760 °C. It is speculated that the granules consist of Zr granules which grow outward after reacting with oxygen to form the ZrO_2 phase on the film surface after annealing. The AFM analysis showed that the annealing temperature has a strong influence on the surface structure of the Zr films deposited on 6H-SiC.

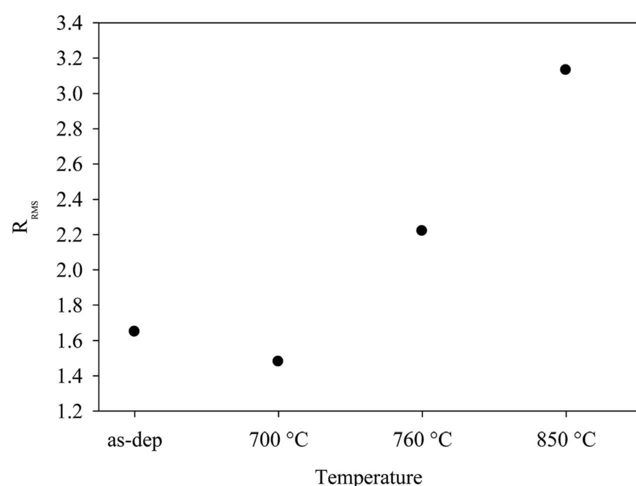

Fig. 7 The influence of annealing temperature on RMS roughness (R_{RMS}) of Zr films deposited on 6H-SiC calculated from the AFM images.

The effective heat of formation (EHF) model was developed to predict the initial phases to form in binary systems by Pretorius *et al.*[20] The binary EHF model is based on thermodynamic parameters (Gibbs free energy of formation, ΔG° or heat of formation, ΔH°) and the concentrations of the reacting species. The effective heat of formation expressed as:

$$\Delta H' = \Delta H^{\text{o}} \times \frac{C}{C^{\text{o}}} \tag{1}$$

where ΔH^{o} is the standard heat of formation in kJ mol^{-1} atom, C is the interface concentration of the element limiting the compound formation and C^{o} is the stoichiometric concentration of the limiting element in the compound obtained from the lowest temperature eutectic in the binary system.

The binary EHF model was extended to ternary systems by Mogilevsky and Gutmanas.[21] In the case of ternary systems, the two dimensional EHF diagrams are replaced by corresponding three dimensional constructions where the tetrahedral replace the binary EHF triangles. From these three dimensional maps, phases favoured to form can be predicted. Prediction of initial phases to form can be performed without knowledge of the location of the lowest temperature eutectic (even if it is known) unlike the case in binary systems. This implies that it is impossible to attribute the initial phase to form to the one having the maximum effective energy of formation.

For the Zr–Si–C ternary system with element Zr and compound SiC as the reacting materials, the possible reaction products are ZrC in the Zr–C section and ZrSi, Zr_2Si, $ZrSi_2$, Zr_5Si_3 in the Zr–Si section of the ternary phase diagram. A 3D projection of the stoichiometric concentration and ΔG^{o} of the reactants, reaction product phases ZrC and Zr_2Si (only this silicide phase used in example here) can be plotted and the regions where the tetrahedral intersect, the effective free energy of Zr_2Si is equal to that of ZrC, given as;

$$\Delta G'_{Zr_2Si} = \Delta G'_{ZrC} \tag{2}$$

where

$$\Delta G'_{Zr_2Si} = \Delta G^{\text{o}}_{Zr_2Si} \times \frac{x_{Si}}{x^{\text{o}}_{Si}} \text{ and } \Delta G'_{ZrC} = \Delta G^{\text{o}}_{ZrC} \times \frac{x_C}{x^{\text{o}}_C} \tag{3}$$

x^{o}_{si} is the stoichiometric concentration of Si in Zr_2Si and x_{si} is the limiting stoichiometric concentration of Si in Zr_2Si. For Zr_2Si in the Zr rich region, elements Si and C are limiting, while for ZrC in the C rich region, elements Si and Zr are limiting. The projection of the effective free energy tetrahedral gives the areas of favourable formation and these are usually close to the line, connecting Zr and SiC, the starting materials. The calculated effective free energy values for the Zr–Si–C system are given in Table 1. The EHF model has been previously applied to metal/SiC systems including Ta/SiC, Ti/SiC and Nb/SiC by Mogilevsky and Gutmanas.[21] These metals form both silicides and carbides with SiC and the initial phases to form in these ternary systems were predicted to good accuracy.

Chen *et al.*[24] provided a complete thermodynamic analysis of the Zr–Si–C system. The Gibbs free energies of formation and the calculated effective free energies of ZrC and Zr silicides

 This journal is © The Royal Society of Chemistry 2016

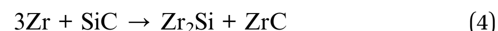

Table 1 Gibbs free energy of formation and of effective free energy of formation for the Zr/SiC system

Phase	ΔG^o (kJ mol^{-1} at.)	$\Delta G'$ (kJ mol^{-1} at.)	MP (°C)
ZrSi	−98.61	−65.74	2203 (ref. 37)
$ZrSi_2$	−70.00	−42.04	1626 (ref. 37)
Zr_5Si_3	−90.87	−66.09	2181 (ref. 37)
Zr_5Si_3C	−34.06	−27.87	—
Zr_2Si	−94.42	−70.89	1926 (ref. 37)
ZrC	−108.21	−72.14	3427 (ref. 38)
SiC	−34.5		2830 (ref. 39)

given in Table 1 and used in Fig. 8(a) have been calculated from SGTE tables[33] and Chen's data. It can be observed that the effective Gibbs energies of formation of ZrSi and Zr_5Si_3 are less than those of ZrC and Zr_2Si phases. Furthermore, the effective Gibbs energy of formation of $ZrSi_2$ and the Zr_5Si_3C ternary phase are considerably less than all the other phases.

The effective free energies of Zr_5Si_3, ZrSi are close to those of Zr_2Si and ZrC but their areas of favourable formation as seen in Fig. 8(b) are far from the Zr–SiC line and therefore cannot be the initial phases to form.

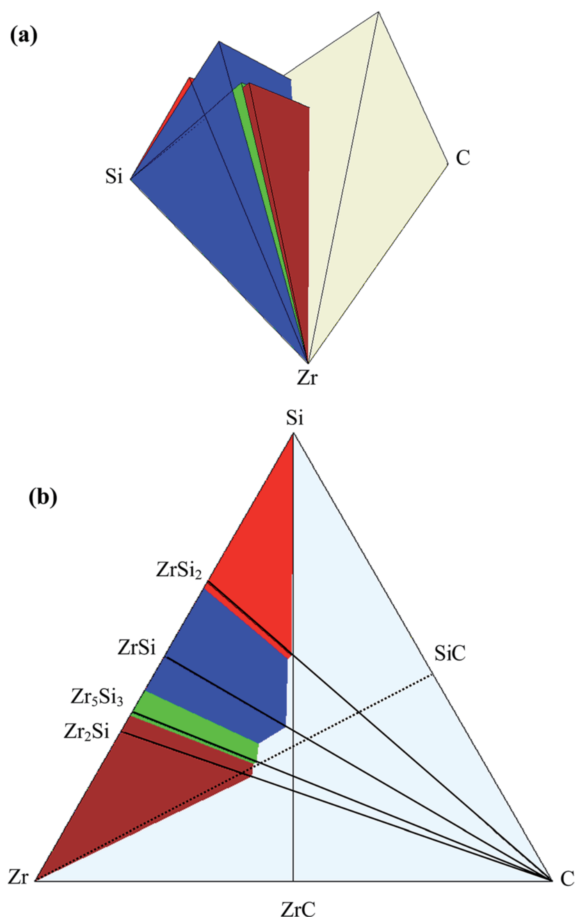

Fig. 8 Ternary EHF diagram of Zr–Si–C system (a) 3-D rendering (b) 2D projection depicting regions of favourable phase formation.

The line connecting Zr and SiC passes through the Zr_2Si and ZrC phase regions and therefore these are the favourable compounds expected to form first according to eqn (4)

$$3Zr + SiC \rightarrow Zr_2Si + ZrC \tag{4}$$

The heat of reaction ΔG_R of eqn (1) is −131.8 kJ mol^{-1}. Since the heat of reaction is negative, the reaction would proceed since the two reactants are not thermodynamically stable. Simultaneous formation of ZrC and Zr_2Si should be expected experimentally to satisfy mass balance. This was observed to experimentally occur in this study. Consequently, the experimental observations agree with the ternary EHF model for initial phase formation.

In metal/SiC reactions, the initial composition near the interface should be close to the metal–SiC connection line in the respective ternary phase diagram. Van Loo *et al.* state that the first nucleated phase should be a ternary compound or a binary phase with extensive solubility of the third element.[18] Therefore, in the Zr/SiC system, the ternary phase $Zr_5Si_3C_x$ is kinetically favoured to form since it takes less time to redistribute elements but this was not observed to be the case in this study.

The as-deposited Zr/SiC sample had to be simulated with a thin intermixed layer with a high concentration of Zr and lower concentrations of Si and C at the Zr layer/SiC interface. The XRD analysis of this sample confirmed the presence of ZrC and Zr_2Si in the as-deposited sample. The existence of these phases was not expected to occur during room temperature deposition. This discrepancy might be attributed to the SiC surface on which the Zr was deposited, being no longer stoichiometric SiC. The RF Ar plasma cleaning process of the SiC substrate created a surface with a disproportionate amount of C atoms since Si and C have different sputtering rates. This preferential etching of silicon from SiC surface leading to the formation of a carbon-rich surface layer by a RF plasma process by low energy (0.5 to 5 keV) argon ion bombardment has been observed to occur before in.[34–36] The deposition of Zr creates an intermixing effect between Zr and C which resulted in the formation of ZrC on the as-deposited sample as observed from XRD results. Transition metals such as W, Mo and Ta have been observed form a thin intermixed layer of carbide and silicide after deposition at room temperature.[36] The formation of ZrC at room temperature has not been previously observed to occur in bulk diffusion couples. The thermodynamic driving force for formation of ZrC is considerably higher than that of Zr silicides. This coupled by the presence of carbon available to react with Zr, results in the formation of the ZrC in the as-deposited sample.

4. Conclusion

Zirconium films were sputter deposited on 6H-SiC substrates. The initial reactions and phases formed, their evolution and surface topography after annealing were analysed by RBS, XRD, SEM and AFM. Observations made by SEM and AFM revealed that the surface morphology of the Zr films prepared by sputter deposition appeared homogeneous and smooth. The films have

a good uniformity with no significant changes in surface morphology at annealing temperature of 700 °C. The R_{RMS} roughness was observed to decrease after annealing from 1.65 nm to 1.48 nm. With increase in annealing temperature, the R_{RMS} values are observed to gradually increase to a maximum value of 3.13 nm due to agglomeration of surface granules on the Zr layer surface leading to the appearance of island clusters. The film annealed at 850 °C is very rough and composed of islands clusters.

In the as-deposited sample, ZrC was the initial phase to form and this occurs during deposition. This indicates the effect of the fabrication technique since ZrC does not form in bulk samples. The Zr/SiC interface was found to be stable up to 700 °C in vacuum. Both silicides and carbides are formed in the Zr/SiC system after annealing at temperatures higher than 700 °C and the reaction zone consists of a mixture of silicides (Zr_2Si, $ZrSi_2$), and carbide (ZrC). The reactions were characterized with slow reaction rates at 700 to 800 °C, which increased considerably indicating rapid reactions at 850 °C which is close to the α to β-Zr transformation temperature. Annealing at 850 °C for 2 h leads to the formation of many and complex phases.

Zr is not in thermodynamic equilibrium with SiC. The difference in the Gibbs' free energies for the possible reactions at the Zr/SiC interface is the thermodynamic driving force which leads to interface reactions which causes a change of the interface structure. A good correlation between the calculated ternary EHF model and experimental data has been obtained. The initial phases formed in this study (ZrC and Zr_2Si) were found to agree with the ternary EHF model. Detailed TEM study of the microstructure at the interface after high temperature annealing is needed to fully understand the reaction mechanism.

Acknowledgements

The authors wish to thank Mr T. Ntsoane and Dr A. Venter from Necsa for their assistance with the XRD analysis.

References

1 G. W. Liu, M. L. Muolo, F. Valenza and A. Passerone, Survey on wetting of SiC by molten metals, *Ceram. Int.*, 2010, **36**, 1177–1188.

2 J. A. Cooper, Critical material and processing issues of SiC electronic devices, *Mater. Sci. Eng., B*, 1997, **44**, 387–391.

3 A. R. Powell and L. B. Rowland, SiC Materials – Progress, Status, and Potential Roadblocks, *Proc. IEEE*, 2002, **90**, 942–955.

4 Y. Zhang, W. J. Weber, W. Jiang, A. Hallén and G. Possnert, Damage evolution and recovery on both Si and C sublattices in Al-implanted 4H-SiC studied by Rutherford backscattering spectroscopy and nuclear reaction analysis, *J. Appl. Phys.*, 2002, **91**, 6388–6395.

5 M. Bhatnagar and B. J. Baliga, Comparison of 6H-SiC, 3C-SiC, and Si for Power Devices, *IEEE Trans. Electron Devices*, 1993, **40**, 645–655.

6 J. B. Malherbe, Diffusion of fission products and radiation damage in SiC, *J. Phys. D: Appl. Phys.*, 2013, **46**, 1–27.

7 N. G. van der Berg, J. B. Malherbe, A. J. Botha and E. Friedland, SEM analysis of the microstructure of the layers in triple-coated isotropic (TRISO) particles, *Surf. Interface Anal.*, 2010, **42**, 1156–1159.

8 J. B. Malherbe, E. Friedland and N. G. van der Berg, Ion beam analysis of materials in the PBMR reactor, *Nucl. Instrum. Methods Phys. Res., Sect. B*, 2008, **266**, 1373–1377.

9 L. L. Snead, T. Nozawa, Y. Katoh, T.-S. Byun, S. Kondo and D. A. Petti, Handbook of SiC properties for fuel performance modeling, *J. Nucl. Mater.*, 2007, **371**, 329–377.

10 R. L. Pearson and T. B. Lindemer, Simulated fission product oxide behaviour in triso-coated HTGR fuel, in *Report ORNL/TM-6741*, Oak Ridge National Laboratory, 1979.

11 E. S. Lyman, The pebble-bed modular reactor (PBMR): safety issues, *Forum Phys. Soc.*, 2001, **30**, 16–19.

12 B. G. Kim, Y. Choi, J. W. Lee, Y. W. Lee, D. S. Sohn and G. M. Kim, Multi-layer coating of silicon carbide and pyrolytic carbon on UO_2 pellets by a combustion reaction, *J. Nucl. Mater.*, 2000, **281**, 163–170.

13 C.-H. Andersson and R. Warren, Silicon carbide fibres and their potential for use in composite materials. Part 1, *Composites*, 1984, **15**, 16–24.

14 K. A. Terrani, J. O. Kiggans and L. L. Snead, Fabrication and preliminary evaluation of metal matrix microencapsulated fuels, *J. Nucl. Mater.*, 2012, **427**, 79–86.

15 Y. A. Chang and C. R. Kao, Application of thermodynamics, phase equilibria and kinetics to *in situ* composite synthesis *via* ternary solid-state displacement reactions, *Pure Appl. Chem.*, 1994, **66**, 1797–1806.

16 J. Porta, P. P. Lo, M. Bonnet, K. Kugele, Z. Alkan, R. Heuss, *et al.*, Coated particle fuel to improve safety, design, economics in water-cooled and gas-cooled reactors, *Prog. Nucl. Energy*, 2001, **38**, 407–410.

17 C. Kamezawa, M. Hirai, M. Kusaka, M. Iwami and J. Labis, Surface analyses of Zr (film)/4H-SiC (substrate) by synchrotron radiation induced-PEEM, *Appl. Surf. Sci.*, 2004, **237**, 607–611.

18 F. J. J. van Loo and A. A. Kodentsov, Interfacial chemistry: reactions in inorganic systems, *Pure Appl. Chem.*, 1998, **70**, 501–508.

19 J. C. Schuster, Physical Chemistry of Ceramic-Metal Interface Formation, *Trans. JWRI*, 1994, **23**, 143–147.

20 R. Pretorius, T. K. Marais and C. C. Theron, Thin film compound phase formation sequence: an effective heat of formation model, *Mater. Sci. Rep.*, 1993, **10**, 1–83.

21 P. Mogilevsky and E. Y. Gutmanas, First phase formation at interfaces: effective heat of formation model for ternary systems, *Mater. Sci. Eng., A*, 1996, **208**, 203–209.

22 T. Fukai, M. Naka and J. C. Schuster, Bonding and interfacial strucures of SiC–Zr joint, *Trans. JWRI*, 1996, **25**, 59–62.

23 K. Bhanumurthy and R. Schmid-Fetzer, Interface reactions between silicon carbide and metals (Ni, Cr, Pd, Zr), *Composites, Part A*, 2001, **32**, 569–574.

24 H. M. Chen, Y. Xiang, S. Wang, F. Zheng, L. B. Liu and Z. P. Jin, Thermodynamic assessment of the C–Si–Zr system, *J. Alloys Compd.*, 2009, **474**, 76–80.

This journal is © The Royal Society of Chemistry 2016

25 E. G. Njoroge, C. C. Theron, J. B. Malherbe and O. M. Ndwandwe, Kinetics of solid-state reactions between zirconium thin film and silicon carbide at elevated temperatures, *Nucl. Instrum. Methods Phys. Res., Sect. B*, 2014, **332**, 138–142.
26 E. G. Njoroge, C. C. Theron, J. B. Malherbe, N. G. van der Berg, T. T. Hlatshwayo and V. A. Skuratov, Surface and interface modification of Zr/SiC interface by swift heavy ion irradiation, *Nucl. Instrum. Methods Phys. Res., Sect. B*, 2015, **354**, 249–254.
27 L. R. Doolittle, Algorithms for the rapid simulation of Rutherford backscattering spectra, *Nucl. Instrum. Methods Phys. Res., Sect. B*, 1985, **9**, 344–351.
28 T. C. Chou, A. Joshi and J. Wadsworth, High temperature interfacial reactions of SiC with metals, *J. Vac. Sci. Technol., A*, 1991, **9**, 1525–1534.
29 G. M. Hood and R. J. Schultz, Tracer diffusion in α-Zr, *Acta Metall.*, 1974, **22**, 459–464.
30 D. K. Aswal, K. P. Muthe, S. Tawde, S. Chodhury, N. Bagkar, A. Singh, *et al.*, XPS and AFM investigations of annealing induced surface modifications of MgO single crystals, *J. Cryst. Growth*, 2002, **236**, 661–666.
31 M. Bouville, D. Z. Chi and D. J. Srolovitz, Grain-boundary grooving and agglomeration of alloy thin films with a slow-diffusing species, *Phys. Rev. Lett.*, 2007, **98**, 1–4.
32 Y. Dao, D. E. Sayers and R. J. Nemanicha, Phase stabilities and surface morphologies of $(Ti_{1-x}, Zr_x)\ Si_2$ thin films on Si(100), *J. Appl. Phys.*, 1995, **78**, 6584–6591.
33 A. T. Dinsdale, SGTE Data for Pure Elements, in *DMA Report No A195*, National Physical Laboratory, Teddington, United Kingdom, 1989.
34 J. B. Malherbe, Sputtering of compound semiconductor surfaces. I. Ion-solid interactions and sputtering yields, *Crit. Rev. Solid State Mater. Sci.*, 1994, **19**, 55–127.
35 J. A. Kalomiros, E. C. Paloura, A. Ginoudi, S. Kennou, S. Ladas, C. Lioutas, *et al.*, Surface modification of α-SiC thin films with *ex situ* hydrogenation, *Solid State Commun.*, 1995, **96**, 735–738.
36 K. M. Geib, C. Wilson, R. G. Long and C. W. Wilmsen, Reaction between SiC and W, Mo and Ta at elevated temperatures, *J. Appl. Phys.*, 1990, **68**, 2796–2800.
37 S. V. Meschel and O. J. Kleppa, Standard enthalpies of formation of some 4d transition metal silicides by high temperature direct synthesis calorimetry, *J. Alloys Compd.*, 1998, **274**, 193–200.
38 E. Rudy, P. Harmon and C. E. Brukl, Ternary Phase Equilibria in Transition Metal–Boron–Carbon–Silicon Systems Part I Related Binary Systems vol. II, Ti–C and Zr–C, in *Technical Report No AFML-TR-65-2*, 1965.
39 J. Narayan, R. Raghunathan, R. Chowdhury and K. Jagannadham, Mechanism of combustion synthesis of silicon carbide, *J. Appl. Phys.*, 1994, **75**, 7252–7257.

This journal is © The Royal Society of Chemistry 2016